Comparison of an Experimental NOAA AVHRR Cloud Dataset with Other Observed and Forecast Cloud Datasets

YU-TAI HOU

General Science Corporation, Laurel, Maryland

KENNETH A. CAMPANA AND KENNETH E. MITCHELL

National Meteorological Center, Washington, D.C.

SHI-KENG YANG

Research and Data Systems, Corporation, Greenbelt, Maryland

LARRY L. STOWE

National Environmental Satellite, Data, and Information Service, Washington, D.C.

(Manuscript received 16 September 1992, in final form 27 April 1993)

ABSTRACT

CLAVR [cloud from AVHRR (Advanced Very High Resolution Radiometer)] is a global cloud dataset under development at NOAA/NESDIS (National Environmental Satellite, Data, and Information Service). Total cloud amount from two experimental cases, 9 July 1986 and 9 February 1990, are intercompared with two independent products, the Air Force Real-Time Nephanalysis (RTNEPH), and the International Satellite Cloud Climatology Project (ISCCP). The ISCCP cloud database is a climate product processed retrospectively some years after the data are collected. Thus, only CLAVR and RTNEPH can satisfy the real-time requirements for numerical weather prediction (NWP) models. Compared with RTNEPH and ISCCP, which only use two channels in daytime retrievals and one at night, CLAVR utilizes all five channels in daytime and three at night from AVHRR data. That gives CLAVR a greater ability to detect certain cloud types, such as thin cirrus and low stratus. Designed to be an operational product, CLAVR is also compared with total cloud forecasts from the National Meteorological Center (NMC) Medium Range Forecast (MRF) Model. The datasets are mapped to the orbits of NOAA polar satellites, such that errors from temporal sampling are minimized. A set of statistical scores, histograms, and maps are used to display the characteristics of the datasets. The results show that the CLAVR data can realistically resolve global cloud distributions. The spatial variation is, however, less than that of RTNEPH and ISCCP, due to current constraints in the CLAVR treatment of partial cloudiness. Results suggest that if the satellite cloud data is available in real time, it can be used to improve the cloud parameterization in numerical forecast models and data assimilation systems.

1. Introduction

The important role of clouds in long-range climate study and in short-range and medium-range forecasting has been recognized over the past several decades by many atmospheric researchers (Manabe 1969; Herman et al. 1980; Ramanathan et al. 1989; Wilson and Mitchell 1986; Stephens and Greenwald 1991). A number of cloud parameterization schemes have since been developed for numerical atmospheric models (e.g., Slingo 1980, 1987; Sundqvist et al. 1989). However, incomplete understanding of cloud physical processes and lack of an accurate three-dimensional description of cloud distributions are still believed to be the major sources of uncertainty in radiative processes affecting model performance. To reduce this uncertainty, the National Meteorological Center (NMC) and other forecast centers are increasing their use of traditional and newly available real-time cloud observations to validate and improve model cloud–radiation parameterizations, as well as improve model initial analyses by the four-dimensional data assimilation of atmospheric fields inferred from cloud observations (e.g., winds, humidity, and cloud water).

An experimental satellite-derived cloud dataset is being developed at NOAA/NESDIS (National Environmental Satellite, Data, and Information Service) to help satisfy these cloud-modeling requirements in real time. The cloud data retrieval system is referred to as the "CLAVR" [cloud from AVHRR (Advanced Very

Corresponding author address: Dr. Yu-Tai Hou, GSC/NMC, National Meteorological Center, Washington, DC 20233.

High Resolution Radiometer)] algorithm. It is a sequential, multispectral decision-tree threshold algorithm using information from NOAA satellites (Stowe 1991; Stowe et al. 1991). The algorithm is based on the following differences between the radiative and physical properties of clouds and the underlying surface: magnitudes of reflected and emitted radiation (contrast), wavelength dependence, and spatial variability. Because CLAVR uses all five channels in daytime retrievals and three channels at night (Stowe et al. 1991), it is better able to detect certain cloud types, such as thin cirrus and low stratus, compared with other available global cloud analyses that commonly use only two channels in daytime and one at night (Schiffer and Rossow 1983; Hamill 1992).

A preliminary evaluation of the CLAVR cloud product has been made for two (1 day) datasets: a winter day, 9 February 1990; and a summer day, 9 July 1986. These two cases were used as test days for initial CLAVR algorithm development and testing. Independent cloud analyses from either the U.S. Air Force Real-Time Nephanalysis (RTNEPH) or the International Satellite Cloud Climatology Project (ISCCP) are used in the evaluation. However, no direct comparisons are made here between ISCCP and RTNEPH because the ISCCP analyses for the case of 1990 were not available at the time of this study and the RTNEPH data for the case of 1986 were not suitably at hand "in house," though the latter are obtainable for follow-up studies from the U.S. Air Force archive described by Zamiska (1986). Data fields from the NMC global analysis and forecast model are also available for comparison. While the initial evaluation is restricted to total cloud amount, additional products such as layered cloud amount, cloud-top temperature and pressure, cloud radiative properties, and cloud type are planned.

The next section briefly describes the cloud datasets used in this study and the choice of spatial and temporal scales for the comparison. Sections 3 and 4 show comparisons among the datasets either with histogram analysis or statistical scores. Section 5 displays a number of two-dimensional cloud maps from the datasets.

2. Datasets

The phase I CLAVR "test" cloud datasets (CLAVR-I) are derived from *NOAA-9* and *NOAA-11* polar-orbiting satellites. They provide global total cloud distributions twice daily, once for ascending segments of the orbits (mostly from daytime retrievals) and once for descending segments (mostly from nighttime retrievals). Day–night retrievals switch at a solar zenith angle of 84.3°. The local equator crossing times are approximately 1400–1600 for the ascending segments of the orbits and 0200–0400 LST for the descending segments. The retrieved cloud information is mapped to a longitude–latitude equal-angle grid of 0.5° resolution. During daytime retrievals, information from all five AVHRR channels (two visible, three infrared) is used, but only infrared channels are available for nighttime retrievals (Stowe et al. 1991). Included in this study are cloud amount maps for both ascending and descending segments on the two test days, or a total of four CLAVR-I cloud datasets.

Over the polar regions, cold snow-covered surfaces pose more difficulties for satellite cloud retrievals (Stowe et al. 1991). In a study of the U.S. Air Force 3D-Nephanalysis (3DNEPH, the predecessor of the current RTNEPH), Henderson-Sellers (1985) noted that the strong temperature inversion over polar regions probably contributes to an apparent underestimate of polar clouds by satellites, relative to estimates made from surface observations. Furthermore, a serious overestimate of antarctic cloud was also noted by Stowe et al. (1989) due probably to the poor specification of surface temperature in the 3DNEPH database. Therefore, for the cloud data intercomparison, all data are restricted to the region between 60°N and 60°S. Where missing data exist in a cloud dataset, data from all of the other datasets are excluded from the comparisons at those locations.

The cloud distribution diagnosed from forecasts made by a research version of NMC's Medium Range Forecast (MRF) Model (Kanamitsu 1989) is also used in the comparison. The model has a horizontal triangular truncation at wavenumber 80 (horizontal resolution of approximately 2°), and has 18 unevenly placed vertical sigma layers. The model cloud prediction scheme is described in detail by Campana (1990), and is a version of that developed by Slingo (1987) for the European Centre for Medium-Range Weather Forecasts (ECMWF). Clouds are parameterized from model variables either as stratiform (primarily model relative humidity, and adjusted in the low-cloud domain by model vertical velocity and lapse rate) or as cumuliform (using convective precipitation rate). Clouds may be one of the three types: low, middle, or high. Their shortwave radiative properties are fixed, different for each cloud type, while the longwave emissivity of high clouds is a function of latitude.

To obtain the necessary MRF cloud data for mapping into satellite orbits, the model radiation (both longwave and shortwave) and cloud parameterizations are computed once at each model hour during a 72-h forecast period. A characteristic of the model forecast is that moisture and relative humidity require a number of forecast hours to reach model equilibrium. This spinup time directly affects the model cloud generation scheme in middle to high latitudes and takes about two model days to complete (Campana 1990). Thus, only the cloud information from the 48–72-h forecasting period is used for the comparisons. The model forecast begins 48 h prior to the desired day, a period long enough to account for much of the model spinup, but short enough so that the forecast is still a reasonable simulation of the atmosphere. MRF cloud data are

collected from the 24 forecast hours that cover either 9 February 1990 or 9 July 1986.

The RTNEPH cloud dataset (Kiess and Cox 1988; Hamill et al. 1992) is an automated global cloud analysis produced routinely by the U.S. Air Force. It provides real-time analyses of cloud amount, cloud type, and cloud height at 48 km (25 n mi) horizontal resolution every 3 h on two hemispheric polar stereographic grids (true at 60° latitude). It is used for the winter case comparison. Much of the information for the RTNEPH cloud analysis comes from the Defense Meteorological Satellite Program (DMSP) measurements; however, conventional observations and limited data from partial orbits of NOAA polar-orbiting satellites are included in certain regions, such as the tropics [less than 5% of the total; J. Pereira (1992), personal communication]. Though the cloud analysis is updated every 3 h, some data points may not change due to lack of more recent observational information. Furthermore, local equatorial crossing times in 1990 are approximately 0600 and 1800 for one of the DMSP satellites, and 0930 and 2130 LST for the other (Hamill et al. 1992). As a result, very little visible channel information can be used because, at these times, the solar elevation is too low to be suitable for reliable cloud detection.

Cloud data from the ISCCP database (Schiffer and Rossow 1983; Rossow et al. 1985) are used for the summer case of 9 July 1986. The ISCCP data contains cloud distribution on a relatively coarse, 250-km equal-area global grid, which may be transformed into an equal-angle grid of 2.5° resolution. Information in the ISCCP cloud database is updated eight synoptic times daily, primarily with retrievals from geostationary satellites, although polar-orbiting satellite data are used to fill gaps predominantly in the polar latitudes.

Each of the four cloud datasets used in this study has its own map projection and time sampling scheme. Unification of horizontal map projection and data time is necessary for proper intercomparisons. An equal-angle latitude–longitude grid with 1° resolution is selected for the comparison, giving a total of 43 200 grid points in the area between 60°N and 60°S. The 0.5° resolution CLAVR-I data are bilinearly interpolated (4 to 1 average) to the new grid. Originally, cloud data from the MRF model are located on a computational grid (unevenly distributed in latitude), having approximately a 2° horizontal resolution. In this case, a linear interpolation method is used to remap model cloud data. Special treatment, however, is made both to avoid spreading of cloud cover near cloud edges[1] and to preserve its area-weighted global mean amount. The RTNEPH cloud data are binned into 1° boxes (60°N–60°S). The average value of each of the boxes is used to represent the cloud fraction in that area. The remapped data are checked against the original data to ensure that the process preserves the global mean amount. The ISCCP cloud data are first transformed from its 2.5° equal-angle projection to a 0.5° grid projection by the replication method described in the ISCCP data documentation (i.e., use the cloud amount in an original 2.5° grid box to represent each of the 25 0.5° subgrid boxes). This preserves large-scale data statistical properties; however, the original coarse gridded data will not contain the high-resolution cloud details of CLAVR-I (see Fig. 9). The finer grid data are then mapped to 1° resolution by bilinear interpolation.

To make these different cloud datasets comparable within a reasonable time window, while avoiding possible errors introduced by time interpolation, we decided to choose a temporal grid defined by the NOAA satellite orbit times carried in the CLAVR-I data. The RTNEPH and ISCCP datasets with 3-h synoptic update time intervals are mapped to within 1.5 h of the NOAA satellite observing time. This mapping method, however, still presents undesirable time differences between CLAVR-I and RTNEPH. The latter uses mainly DMSP satellites with local observation times 4–5 h away from the NOAA satellite sampling times (Hamill et al. 1992). More discussion on this issue is given later. The MRF model cloud dataset, which has a 1-h time interval, is mapped to the NOAA satellite observing time within half an hour.

3. Cloud distributions—Histogram analysis

Figure 1 shows histograms of global total cloud distributions for ascending segments of the orbit for (a) 9 February 1990 and (b) 9 July 1986, and descending segments of the orbit for (c) 9 February 1990 and (d) 9 July 1986. The fraction of cloud cover is categorized by a 0.1 (i.e., 10%) interval, except that a 0.05 (or 5%) level is used at the clear-sky and overcast ends. In the figure, cloud distributions from the CLAVR-I, RTNEPH, ISCCP, and MRF model are labeled as CLV, RTN, ISC, and MRF, respectively. The daytime satellite cloud data are more reliable than nighttime because visible channel information is included in the cloud retrieval. Thus, most comparisons presented in this study will emphasize the ascending cases.

The appearance of a cloud distribution histogram is a function of the resolution of observations. At two extreme cases, for example, the cloud histogram will show only two spikes at clear and complete cloudy conditions for point observations, or will show one spike peaked at about 0.5 value for global mean observations. In general, satellite-observed cloud histograms are found between the two extreme examples, and commonly show a U-shaped distribution. In the

[1] The special treatment used in the MRF model reduces the spreading of cloud data whenever only one or two of the four grid points surrounding the desired location have cloud fraction greater than zero. The requirement is that the interpolated location must be within a specified radius of the cloud-covered points to be influenced by these points.

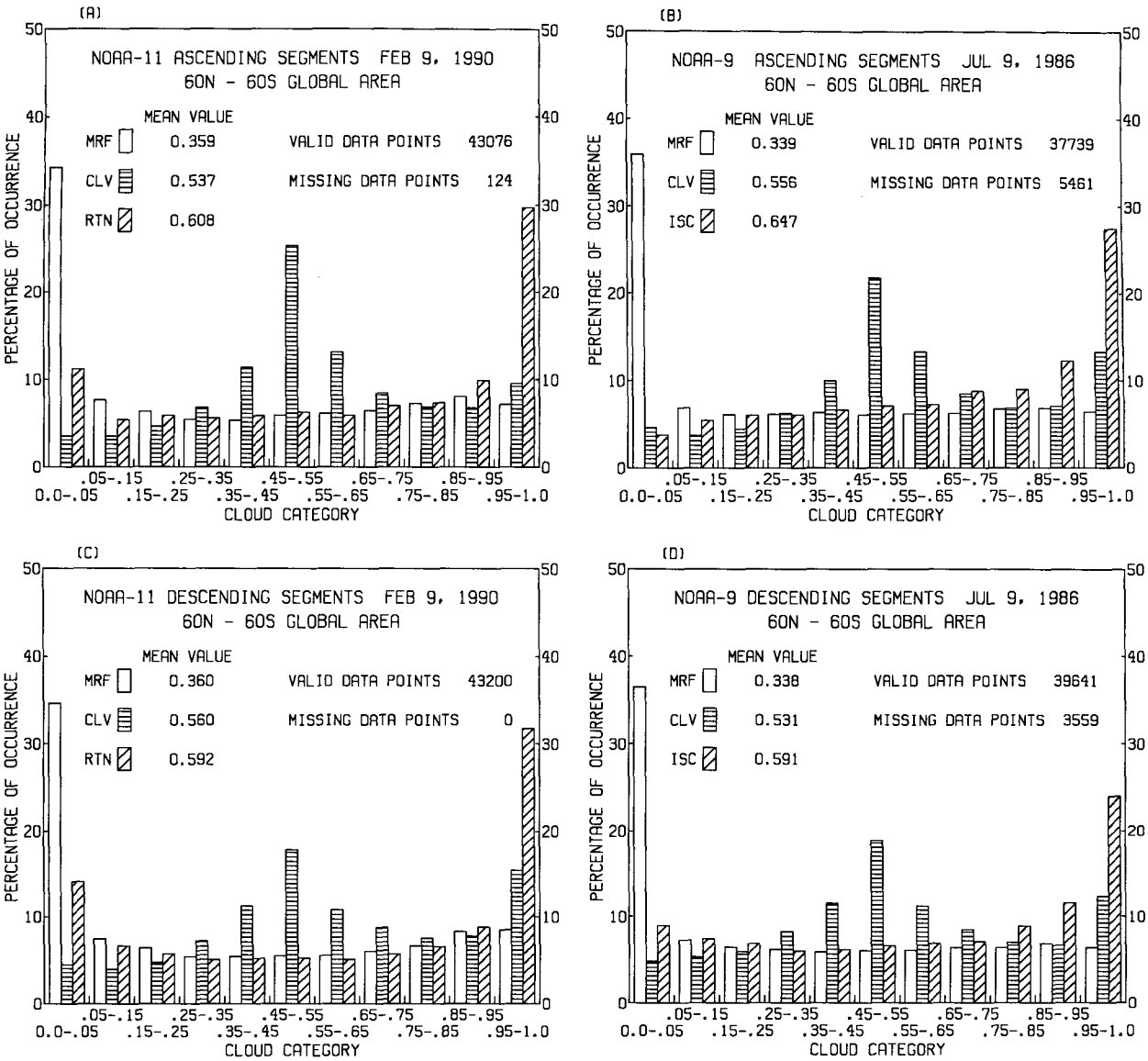

FIG. 1. Histograms of global (60°N–60°S) total cloud distributions. Data for MRF model, CLAVR, RTNEPH, and ISCCP are labeled as MRF, CLV, RTN, and ISC, respectively. Data are mapped on: (a) ascending segments of the orbits of 9 February 1990, (b) ascending segments of the orbits of 9 July 1986, (c) descending segments of the orbits of 9 February 1990, and (d) descending segments of the orbits of 9 July 1986. Mean values give area-weighted mean cloud amounts for the corresponding datasets.

figure, each cloud dataset displays a unique cloud amount distribution histogram. All the datasets show departures from the U-shaped histogram distribution. The MRF model cloud data are skewed toward the cloud-free condition (cloud fraction less than 0.05), indicating that the current model cloud parameterization scheme generates too little cloud cover. Almost 35% of the grid points are covered by little or no clouds, and less than 7% of these are covered completely by clouds (cloud fraction greater than 0.95).

The CLAVR-I cloud amount distribution, on the other hand, peaks in the center of the diagram, at approximately 0.5 cloud fraction. The CLAVR-I algorithm is primarily designed to separate cloud-free AVHRR GAC (global area coverage) pixels from all others. To estimate cloud amount, cloud fractions of 0%, 50%, and 100% are assumed, respectively, for each of the three cloud classifications (cloud-free, mixed cloudy, and cloudy) assigned to each of the 2×2 arrays of GAC pixels (Stowe et al. 1991). As seen in the figure, more than 20% of the grid points have cloud fraction in the range of 0.45–0.55, in contrast to less than about 8% of total occurrences displayed in this range by the other cloud datasets. This occurs because "mixed cloudy" is the predominant classification from the CLAVR-I algorithm. Future phases of the CLAVR al-

gorithm will incorporate energy balance methods (e.g., Coakley and Baldwin 1984) between cloudy and clear pixel radiances and time series analyses of previous day's clear-sky radiance statistics to provide a very precise separation of these mixed-cloudy arrays into a clear, partly cloudy, or cloudy classification for each pixel.

The RTNEPH total cloud amount distributions shown in panels (a) and (c) of Fig. 1 display a bias toward the overcast condition, with more than 30% of the global total occurrences having cloud fraction greater than 0.95. This may result from the U.S. Air Force's design philosophy, which attempts to maximize the probability of detecting cloud (Hamill et al. 1992). The ISCCP cloud amount distributions shown in panels (b) and (d) of the figure display a pattern similar to the RTNEPH data, except for slightly lower frequencies of occurrence at both the high and low ends of the cloud fraction scale. Considering the differences in spatial resolution and season, RTNEPH and ISCCP datasets are generally in good agreement. Area-weighted mean values of global total cloud amount are also shown in the figures for each of the comparison cases. The MRF model cloud data produces global mean cloud values less than 0.36,[2] while the CLAVR-I data produces global mean cloud values in the range of 0.53–0.56. On the other hand, the values of global-mean cloud fraction are between 0.59 and 0.65 for the RTNEPH cloud data and the ISCCP cloud data.

Each cloud dataset also has different cloud amount distributions over land and ocean regions. For example, for ascending segments of the orbit, Figs. 2a and 2c show cloud amount distribution histograms over land and ocean, respectively, for 9 February 1990, and Figs. 2b and 2d show similar histograms for the case of 9 July 1986. In general, all the cloud datasets show a tendency for greater cloud cover over ocean than over land. The three satellite cloud distributions show more overcast conditions and less cloud-free conditions over ocean than over land. For MRF model clouds, differences in cloud coverage between ocean and land are more evenly spread over all cloud fraction categories. However, significantly less cloud-free conditions are observed over the oceans. Regardless of differences in cloudiness, satellite cloud-retrieval algorithms are themselves different over land and ocean backgrounds. These differences suggest that improving a model cloud scheme (tuning), based on real-time satellite data, should be done separately for land and ocean.

4. Cloud statistical scores

To compare statistical characteristics of the cloud distribution for the four cloud datasets, we adapt and extend the computation of cloud comparison skill scores applied at Air Force Global Weather Central (AFGWC) (Trapnell 1992). First, a series of contingency tables (or matrices) and chance tables are calculated for each pair of cloud datasets being compared. Each entry in a contingency table (or a chance table) represents the number of occurrences of cloud (or the chance of cloud occurrence in the chance table) in 1 of 11 cloud fraction categories for each set. In addition to a global region (60°N–60°S), tables are presented for a set of somewhat arbitrarily selected regions in order to assess statistical characteristics associated with changes in latitude, in scene background (land, ocean), and in geographic regions favoring formation of certain cloud types. From the tables, comparison skill scores are then calculated. We use seven scores to show statistical characteristics of cloud datasets. Six of them are selected from Trapnell (1992), and the seventh, the S_{-60} score, is added here as a natural counterpart to one of the six. Considering the lack of accessibility of the cited report, and the lack of an in-depth explanation of scores therein, we include a detailed description of the scoring system in the Appendix.

Tables 1–4 show selected comparison scores for several specified regions for ascending segments for 9 February 1990 and 9 July 1986, and descending segments for 9 February 1990 and 9 July 1986, respectively. The S_{20} score gives an estimate of how well two cloud datasets agree. It is the percent of points where the cloud amount in the two cloud fields differ by less than approximately 20% (i.e., percent of agreement). The score value ranges from 0 to 1. The larger the score, the better the agreement. The S_{-60} score, on the other hand, gives an estimate of how poorly the cloud distributions agree. It is the percent of points where the cloud amount in the two cloud fields differs by more than 60% (i.e., percent of disagreement). With the score value ranging from zero to one, a large S_{-60} value indicates large disagreement. The bias score S_{bias} is used to compare overall cloud amounts between two cloud datasets. A large value (either positive or negative) indicates that there is a large difference in overall cloud amount. The sign of S_{bias} score shows the direction of the overall bias. Another very useful score is called the Heidike score S_h. The score value, ranging from 0 to 1, measures how closely two compared cloud datasets are related to each other. The larger the value of S_h, the less likely it is that the two cloud datasets are statistically independent of each other. A large S_h score usually implies that most of the other scores will indicate favorable agreement between the datasets. Three additional scores are included in the table. They are the root-mean-square (rms) error S_{rms}, the mean absolute error S_{abs}, and the correlation score S_{corr}, respectively. Since these are commonly used in many other applications with the same statistical meanings, no further descriptions are given here.

Scores shown in Tables 1–4 consist of results from ascending and descending segments of the orbit for

[2] The global-mean cloud value of the current operational T126 model is approximately 0.42, a value still too low.

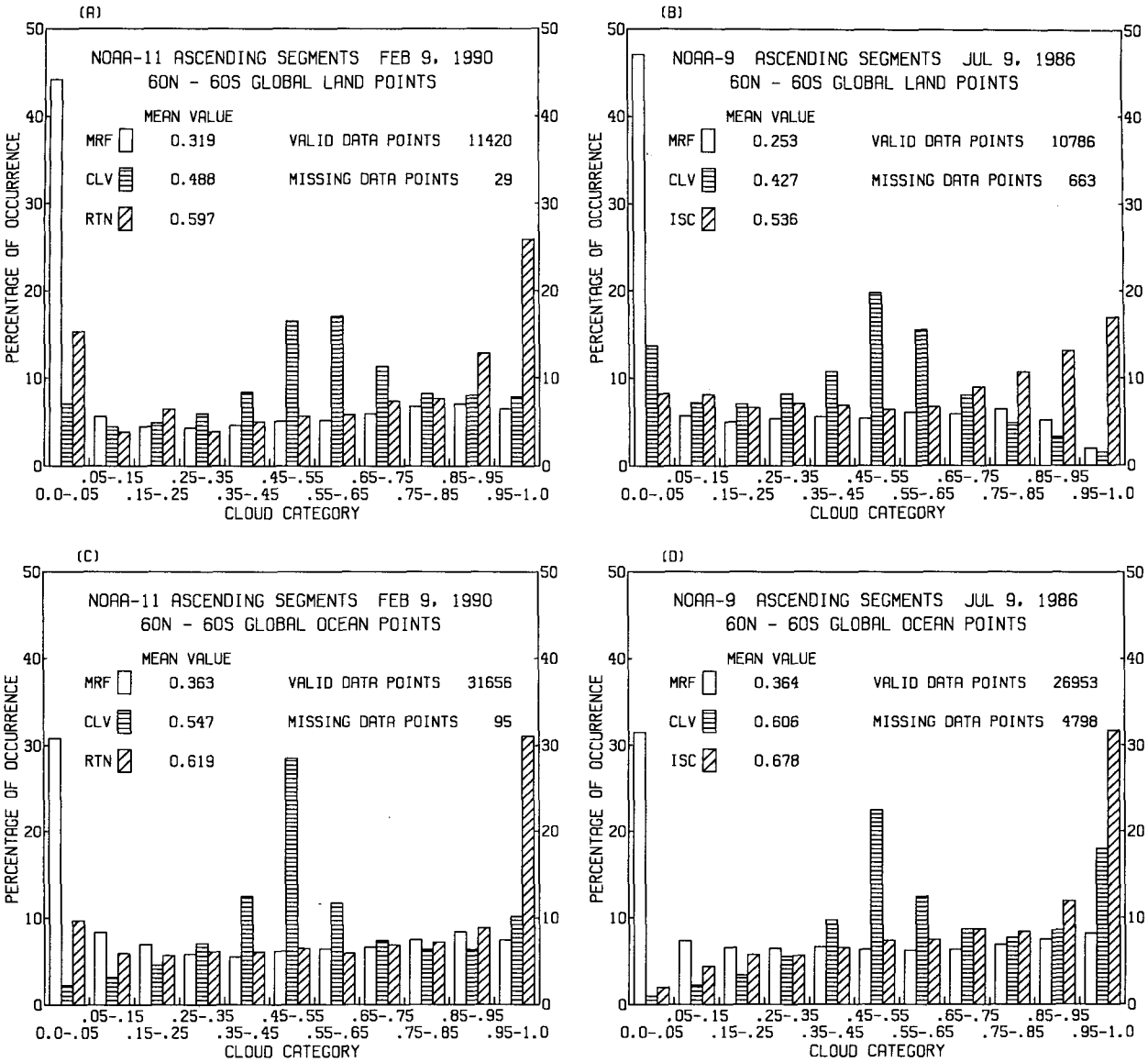

FIG. 2. Histograms of global (60°N–60°S) total cloud distributions. Data for MRF model, CLAVR, RTNEPH, and ISCCP are labeled as MRF, CLV, RTN, and ISC, respectively. Data are mapped on: (a) land areas of ascending segments of 9 February 1990, (b) land areas of ascending segments of 9 July 1986, (c) ocean areas of ascending segments of 9 February 1990, and (d) ocean areas of ascending segments of 9 July 1986.

both the winter case of 9 February 1990 (RTNEPH, CLAVR-I, and MRF datasets) and the summer case of 9 July 1986 (ISCCP, CLAVR-I, and MRF datasets). In each of the cases, three cloud datasets are compared to each other in pairs. For each pair, statistical scores are calculated over the global region. Additionally, scores for two smaller regions are given in the table, which shows relatively good and bad examples of agreement.

Generally speaking, results from comparisons of the CLAVR-I cloud data to either the RTNEPH cloud data or the ISCCP cloud data [section (a) in the tables] are better than results from comparisons of the MRF model clouds to any of the observational cloud databases [sections (b) and (c) in the tables]. In the global region, for instance, values of S_{20} score range from 0.547 to 0.677 for comparisons between the CLAVR-I cloud data and the RTNEPH or ISCCP data. Those values are higher than the 0.378–0.426 score values obtained from model cloud comparisons with any of the observational cloud databases. One of the main reasons for the low MRF scores is attributed to the large amount of clear sky in the forecast model. The S_{20} score values associated with the CLAVR-I cloud data, however,

TABLE 1. Selected statistical scores computed from pairwise comparisons among the CLAVR, RTNEPH, and MRF model total cloud datasets. Data are mapped on *NOAA-11* ascending segments of the orbits of 9 February 1990. For each comparison pair, scores are computed over global area (60°N–60°S). Scores for two selected smaller regions are also included to show examples of relatively good and bad comparisons.

(a) RTNEPH vs CLAVR

Score	Global	Europe	Western North America
S_{20}	0.573	0.638	0.422
S_{-60}	0.062	0.037	0.269
S_{rms}	0.304	0.263	0.452
S_{bias}	0.062	0.067	−0.233
S_{abs}	0.234	0.225	0.361
S_{corr}	0.547	0.591	0.242
S_h	0.334	0.362	0.141

(b) MRFT80 vs CLAVR

Score	Global	Australia	East Asia
S_{20}	0.402	0.495	0.271
S_{-60}	0.188	0.118	0.454
S_{rms}	0.412	0.349	0.549
S_{bias}	−0.173	−0.114	−0.379
S_{abs}	0.335	0.274	0.471
S_{corr}	0.255	0.430	0.113
S_h	0.113	0.221	0.019

(c) MRFT80 vs RTNEPH

Score	Global	Western North America	Tropical Oceans
S_{20}	0.416	0.560	0.377
S_{-60}	0.311	0.211	0.329
S_{rms}	0.488	0.404	0.509
S_{bias}	−0.235	−0.171	−0.238
S_{abs}	0.380	0.287	0.407
S_{corr}	0.249	0.532	0.110
S_h	0.124	0.311	0.050

show only moderately good agreement with the other observed cloud databases, due to the fact that cloud fractions from the CLAVR-I algorithm are heavily biased toward 0.5 from frequently occurring mixed-pixel array classifications. Nevertheless, the S_{-60} scores suggest that the geographical location of clouds detected by the CLAVR-I algorithm is generally in excellent agreement with the other observations. In contrast, the S_{-60} scores are much higher in those comparisons with model-generated clouds, implying that model clouds do not match well with the satellite-derived values. Despite the fact that CLAVR-I clouds have a different cloud amount distribution than either the RTNEPH or ISCCP datasets (recall Figs. 1 and 2), values of the S_{bias} score are quite small for most of the cases. On the other hand, negative score values prevail when comparing model clouds with the other datasets, showing that the current model cloud scheme severely underestimates cloud amount. Values of S_{rms} and S_{abs} are relatively large for the MRF model cloud data comparisons, which, in general, supports the preceding discussion. When comparing data between RTNEPH and CLAVR-I, calculated values for the global region are generally 0.5 or better for S_{corr}, and 0.3 or better for S_h. Even higher scores are yielded when comparing the ISCCP cloud data to the CLAVR cloud data, resulting in corresponding score values of 0.7 and 0.46. Although these scores are significantly lower than the ideal values of one, they have twice the magnitudes obtained in comparisons involving the MRF model cloud data. Despite the fact that neither the RTNEPH nor the ISCCP database represents absolute "truth," the comparison indicates that the CLAVR-I data is in reasonable agreement with these independent cloud datasets. Future phases of the CLAVR development, which will separate mixed-pixel classification into a

TABLE 2. Selected statistical scores computed from pairwise comparisons among the CLAVR, ISCCP, and MRF model total cloud datasets. Data are mapped on *NOAA-9* ascending segments of the orbits of 9 July 1986. For each comparison pair, scores are computed over global area (60°N–60°S). Scores for two selected smaller regions are also included to show examples of relatively good and bad comparisons.

(a) ISCCP vs CLAVR

Score	Global	Eastern Pacific	Western North America
S_{20}	0.677	0.813	0.570
S_{-60}	0.021	0.005	0.027
S_{rms}	0.244	0.187	0.272
S_{bias}	0.092	−0.016	0.183
S_{abs}	0.185	0.141	0.226
S_{corr}	0.700	0.788	0.568
S_h	0.465	0.669	0.209

(b) MRFT80 vs CLAVR

Score	Global	Central Asia	Indian Ocean
S_{20}	0.422	0.591	0.327
S_{-60}	0.185	0.082	0.262
S_{rms}	0.408	0.302	0.468
S_{bias}	−0.179	−0.101	−0.270
S_{abs}	0.326	0.224	0.391
S_{corr}	0.307	0.462	0.079
S_h	0.132	0.298	0.044

(c) MRFT80 vs ISCCP

Score	Global	Europe	Southern Atlantic
S_{20}	0.378	0.464	0.326
S_{-60}	0.322	0.219	0.446
S_{rms}	0.494	0.428	0.579
S_{bias}	−0.293	−0.299	−0.409
S_{abs}	0.396	0.326	0.472
S_{corr}	0.258	0.549	0.114
S_h	0.092	0.222	0.018

TABLE 3. Selected statistical scores computed from pairwise comparisons among the CLAVR, RTNEPH, and MRF model total cloud datasets. Data are mapped on *NOAA-11* descending segments of the orbits of 9 February 1990. For each comparison pair, scores are computed over global area (60°N–60°S). Scores for two selected smaller regions are also included to show examples of relatively good and bad comparisons.

(a) RTNEPH vs CLAVR

Score	Global	Australia	Eastern North America
S_{20}	0.547	0.604	0.453
S_{-60}	0.100	0.066	0.250
S_{rms}	0.335	0.291	0.439
S_{bias}	0.022	0.022	−0.127
S_{abs}	0.252	0.214	0.336
S_{corr}	0.492	0.666	0.202
S_h	0.301	0.391	0.098

(b) MRFT80 vs CLAVR

Score	Global	Europe	East Asia
S_{20}	0.407	0.498	0.287
S_{-60}	0.211	0.180	0.490
S_{rms}	0.430	0.376	0.607
S_{bias}	−0.193	−0.036	−0.400
S_{abs}	0.343	0.288	0.510
S_{corr}	0.281	0.478	0.031
S_h	0.125	0.248	0.006

(c) MRFT80 vs RTNEPH

Score	Global	Western North America	Tropical Atlantic
S_{20}	0.422	0.551	0.311
S_{-60}	0.321	0.220	0.457
S_{rms}	0.492	0.410	0.579
S_{bias}	−0.215	−0.104	−0.266
S_{abs}	0.381	0.289	0.482
S_{corr}	0.250	0.430	−0.152
S_h	0.128	0.262	−0.067

precise spectrum of cloud fraction, may help to reduce the difference.

Over the two smaller regions, scores change greatly from "good" to "bad." For instance, in section (a) of Table 1, comparison of the RTNEPH to the CLAVR-I cloud data over the European region shows that the S_{20}, S_{-60}, S_{bias}, and S_{corr} scores are all in the good range of 0.638, 0.037, 0.067, and 0.591, respectively. This may result from large areas of layered cloud. Over the western part of North America, however, most of the scores are poor, especially for the S_{-60} and S_{bias} scores. Figure 3a shows cloud distribution histograms over this region for the case of 9 February 1990. As seen in the figure, most of the CLAVR-I cloud data are in large cloud amount categories (cloud fraction greater than 0.5), whereas a considerable portion of the RTNEPH data is defined as clear sky or near-clear sky. Note that better agreement exists between the RTNEPH data and the MRF model data. Figure 3b shows another example over the same region but for the summer case of 9 July 1986. Comparisons among CLAVR-I, ISCCP, and MRF model cloud datasets display three different cloud amount distributions, which act to degrade the statistical scores. Differences generally are greater for comparisons involving the MRF model clouds. As shown in Tables 1–4, scores related to the model cloud data in some "bad" examples are so poor that the S_h value indicates that the two referenced cloud distributions are almost totally unrelated (e.g., S_h score less than 0.1).

Further inspection of the tables shows that the CLAVR-I cloud distribution agrees better with the ISCCP distribution than the RTNEPH distribution. As an example, correlations between ISCCP clouds and CLAVR clouds are fairly high, giving S_{corr} values around 0.7 or higher, in contrast to a value less than

TABLE 4. Selected statistical scores computed from pairwise comparisons among the CLAVR, ISCCP, and MRF model total cloud datasets. Data are mapped on *NOAA-9* descending segments of the orbits of 9 July 1986. For each comparison pair, scores are computed over global area (60°N–60°S). Scores for two selected smaller regions are also included to show examples of relatively good and bad comparisons.

(a) ISCCP vs CLAVR

Score	Global	Northern midlatitude land	Southern Atlantic
S_{20}	0.669	0.757	0.571
S_{-60}	0.031	0.016	0.035
S_{rms}	0.254	0.211	0.284
S_{bias}	0.060	0.027	0.118
S_{abs}	0.190	0.152	0.214
S_{corr}	0.697	0.795	0.282
S_h	0.472	0.595	0.146

(b) MRFT80 vs CLAVR

Score	Global	Central Asia	Indian Ocean
S_{20}	0.406	0.594	0.325
S_{-60}	0.191	0.152	0.219
S_{rms}	0.414	0.354	0.456
S_{bias}	−0.198	−0.121	−0.233
S_{abs}	0.334	0.248	0.381
S_{corr}	0.299	0.477	0.038
S_h	0.120	0.304	0.012

(c) MRFT80 vs ISCCP

Score	Global	Europe	Indian Ocean
S_{20}	0.426	0.589	0.305
S_{-60}	0.293	0.153	0.388
S_{rms}	0.472	0.349	0.536
S_{bias}	−0.241	−0.088	−0.352
S_{abs}	0.366	0.243	0.447
S_{corr}	0.291	0.451	0.114
S_h	0.131	0.284	0.024

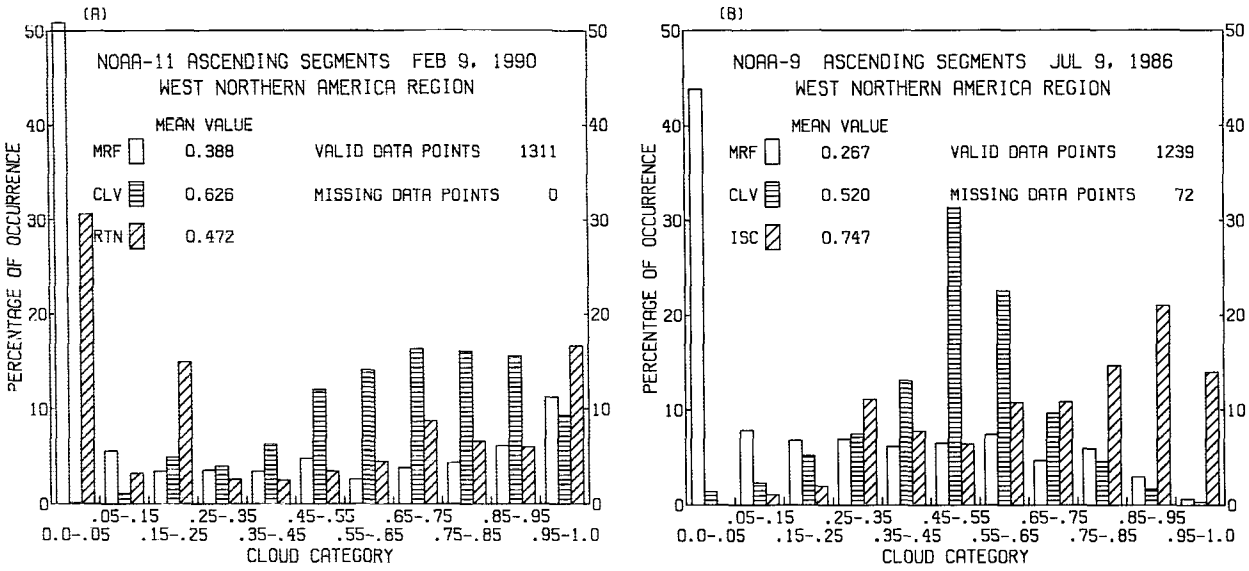

FIG. 3. Histograms of total cloud distributions over the western part of the North American region. Data for MRF model, CLAVR, RTNEPH, and ISCCP are labeled as MRF, CLV, RTN, and ISC, respectively. Data are mapped on: (a) ascending segments of 9 February 1990, and (b) ascending segments of 9 July 1986.

0.6 for the correlation with RTNEPH clouds. A possible explanation for the differences in score values is satellite observation time. Except for relatively few conventional observation points, most RTNEPH observations come from DMSP polar-orbiting satellites that typically have 0600–1800 or 0930–2130 local crossing times and rarely coincide with the data's assigned synoptic times (Hamill et al. 1992). ISCCP data contains cloud information mostly from 3-h geostationary satellites with some data from NOAA polar-orbiting satellites to fill gaps. As a result, the CLAVR-I cloud distribution, which comes solely from NOAA afternoon polar satellites, agrees better with the ISCCP cloud distributions than with RTNEPH data.

5. Two-dimensional cloud distributions

Figures 4 and 5 show maps of total cloud distribution for ascending segments of the orbit on 9 February 1990 and 9 July 1986,[3] respectively. Panel (a) displays cloud amount from the CLAVR cloud dataset, panel (b) from the RTNEPH (or ISCCP), and panel (c) from the MRF model. As expected from the statistical analyses, when CLAVR is compared to the RTNEPH (or ISCCP) cloud distribution, it shows less spatial variability, especially over tropical latitudes. Nevertheless, locations of the most prominent cloud structures in the two satellite-retrieved distributions coincide well with each other, resulting in very small S_{-60} scores in Tables 1–4. Despite less cloudiness over most of the globe by comparison, the MRF model cloud scheme generates reasonably well defined cloud patterns in some regions, especially along the midlatitude storm tracks. Thus we believe that further improvement to the model cloud parameterization can be made through tuning it with a set of cloud observations. Disagreements are also obvious in other regions, especially in low latitudes where model convective clouds become dominant. There, the MRF model clouds do not show large-scale organized cloud patterns. In the current MRF model cloud scheme, there are two types of generation mechanisms (Campana 1990). Stratiform clouds are diagnosed from the model moisture distribution, which generally follows the model's large-scale airmass movement. Convective clouds, on the other hand, are computed from the model convection scheme (Kanamitsu et al. 1989), which depends strongly on the local surface conditions and the static stability of the air mass within a vertical column. The model cloud scheme allows only one type of cloud per model point, and the convective mechanism takes precedence over the stratiform one. Thus, the model convective cloud clusters prevail over low-latitude regions, where the localized convection process is usually very active.

Figures 6–8 show some detailed examples of the three cloud data distributions over different regions of the Pacific Ocean. Figure 6 displays clouds over the northern midlatitude Pacific Ocean. In the figure, all

[3] Two missing segments of satellite orbit are found in the 9 July 1986 display (Fig. 5). The one crossing the Atlantic and northern Africa is from the CLAVR-I dataset, which also masks out the same area in other datasets with mapping processes. The other missing segment (crossing the Pacific Ocean) comes from ISCCP data. Data points within these areas are eliminated from comparisons.

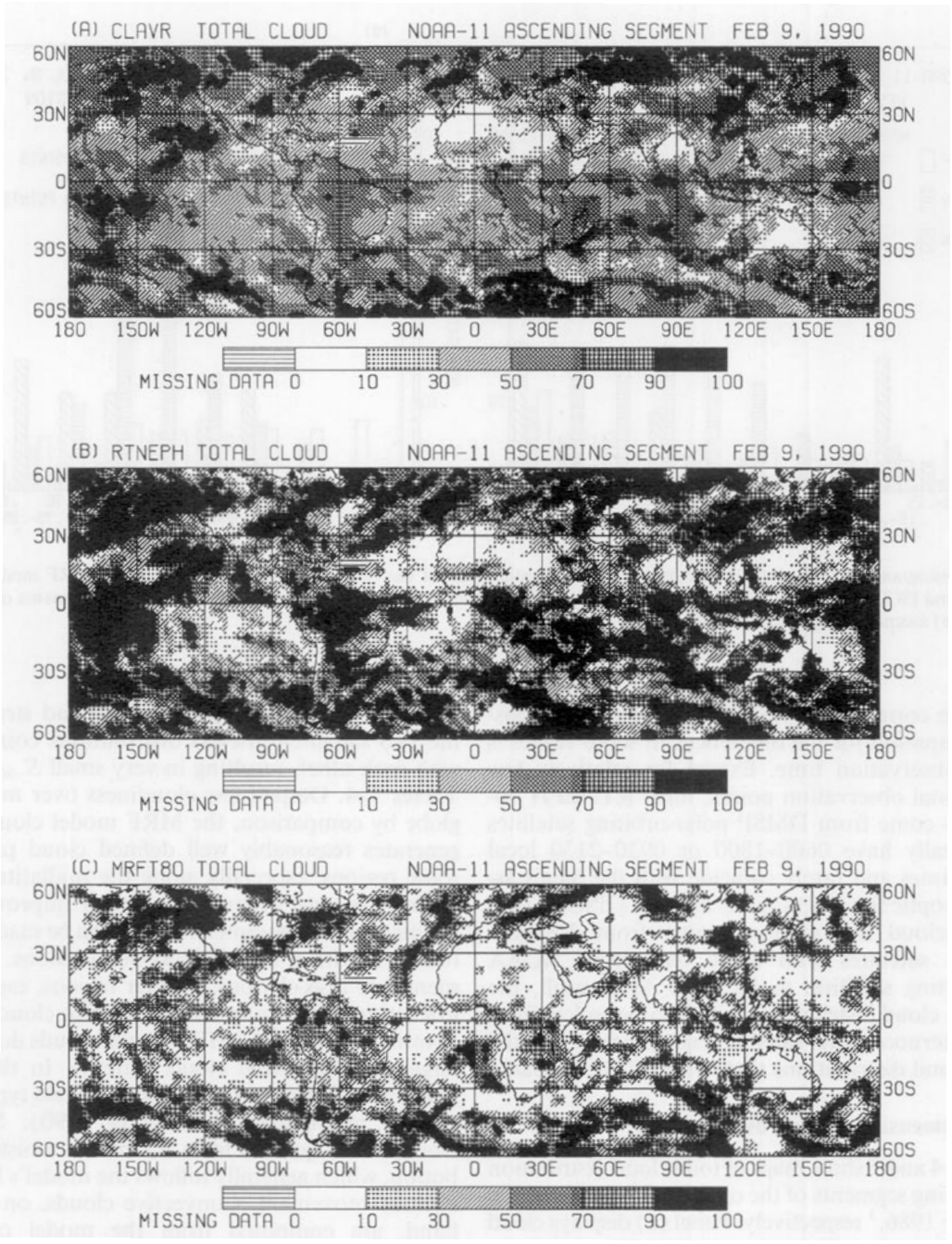

FIG. 4. Comparisons of global (60°N–60°S) total cloud amount distribution. (a) CLAVR total cloud distribution, (b) RTNEPH total cloud distribution, and (c) MRF model total cloud distribution. Data are mapped on *NOAA-11* satellite ascending segments of 9 February 1990.

three show large frontal cloud systems in the eastern part of the ocean. The shape and location of the cloud systems produced by the MRF model cloud generation scheme match quite well with the other two satellite observations. In the central and western parts of the northern Pacific, both the MRF and CLAVR-I clouds display less cloudiness than the RTNEPH. Nevertheless, the agreement between the MRF model and satellite observations is still encouraging. Figure 7 shows a similar comparison for the southern Pacific Ocean. Again, the MRF model cloud scheme compares favorably with observations in predicting large-scale cloud structures. In fact, clouds from the model present an amazingly look-alike large-scale wave pattern across the southern Pacific Ocean, although agreement with observations is less over the western third of the area.

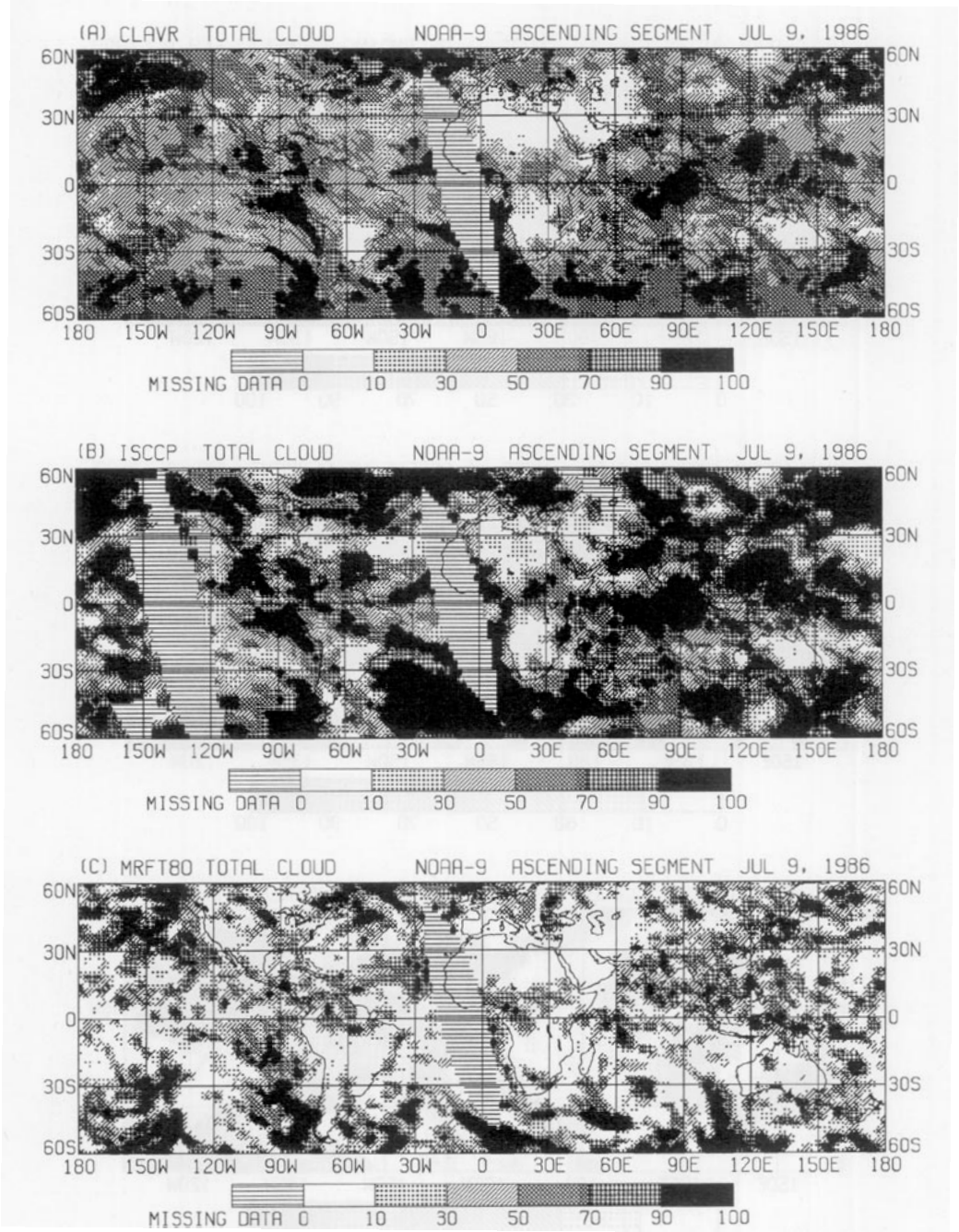

FIG. 5. Comparisons of global (60°N–60°S) total cloud amount distribution. (a) CLAVR total cloud distribution, (b) ISCCP total cloud distribution, and (c) MRF model total cloud distribution. Data are mapped on *NOAA-9* satellite ascending segments of 9 July 1986.

Even though model clouds agree well in cloud pattern, this does not necessarily result in good comparison scores. For example, over the southern Pacific Ocean, where the model cloud scheme appears quite reasonable, comparison between the model data and the RTNEPH data yields S_{20}, S_{-60}, S_{rms}, and S_{corr} scores of 0.448, 0.272, 0.453, and 0.257, respectively. In contrast, comparison between the two satellite cloud databases yields score values of 0.579, 0.049, 0.285, and 0.551, respectively.

Over the tropical Pacific Ocean (Fig. 8), however, agreement between cloud datasets becomes dramatically worse. Though the CLAVR-I cloud map shows less contrast than the RTNEPH cloud map, the similarities in large-scale cloud distribution can still be seen. On the other hand, the MRF model cloud scheme is

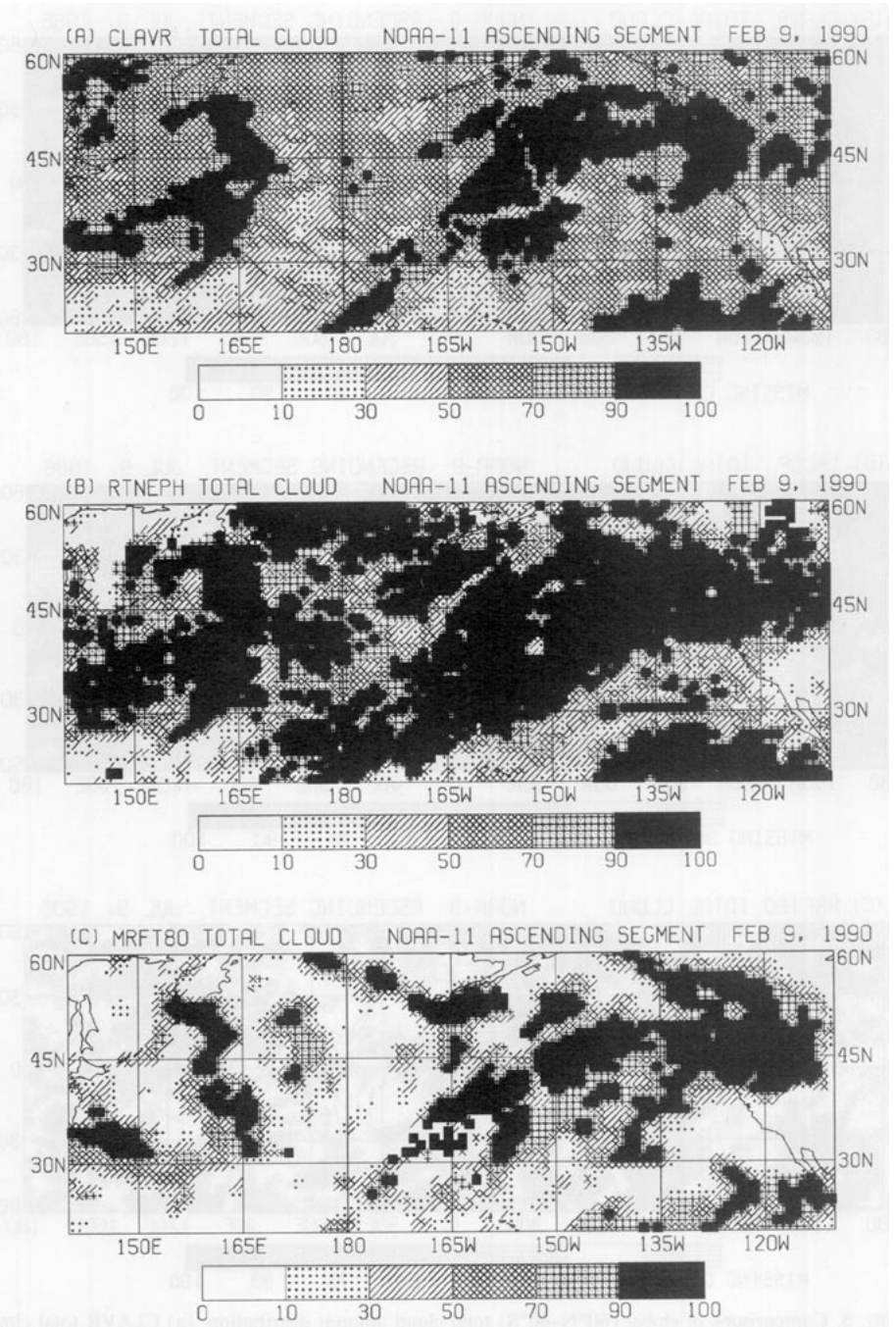

FIG. 6. Similar to Fig. 4 but for the northern midlatitude Pacific region.

not able to produce a similar cloud distribution pattern. Clouds from the model become scattered clusters, diagnosed from model convective processes. Despite the overall underestimate of cloud amount by the MRF model, these areas that strongly disagree will certainly be a major reason for degraded comparison scores (Tables 1–4).

Figure 9 shows an example for 9 July 1986 over the eastern Pacific region. Some missing data points are found in the ISCCP cloud database (mainly west of 120°W), but that does not affect the following discussion. Despite the fact that the ISCCP data has a coarser horizontal resolution (2.5°) than the CLAVR-I data, comparison of the two satellite cloud datasets shows that cloud patterns and locations are in good correspondence, except over the western United States. Although the CLAVR-I cloud map shows less spatial variability, the comparison scores are impressive, giving

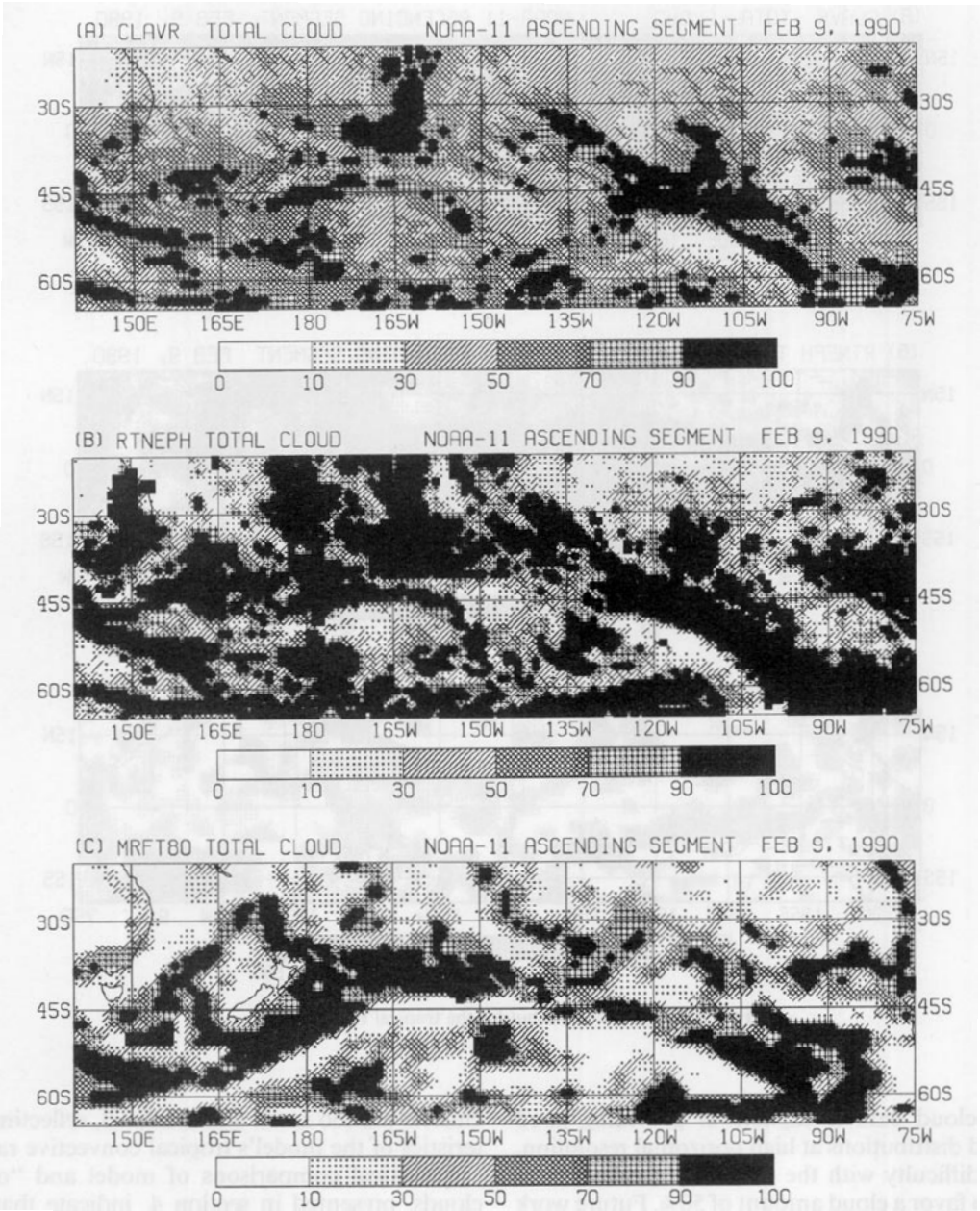

FIG. 7. Similar to Fig. 4 but for the southern midlatitude Pacific region.

S_{20}, S_{60}, S_{rms}, S_{bias}, and S_{corr} of 0.813, 0.005, 0.187, −0.016, and 0.788, respectively.

In contrast, the MRF model clouds compare less favorably. Over the southern Pacific, where the model's stratiform cloud mechanism is dominant, large-scale cloud structures are present. The patterns and locations of those cloud organizations, however, are different from the satellite observations, suggesting that further improvement in the parameterization of model stratus clouds is needed. The deficiency in large-scale cloud pattern is considered to be caused mainly by imperfections in both the initial model conditions and the large-scale model airmass flows and distributions. Again, over the intertropical convergence zone (ITCZ) and Mexico, model convective clouds become scattered clusters, not at all like those large cloud systems shown in the satellite retrievals.

6. Concluding remarks

Comparisons of the experimental NOAA/NESDIS CLAVR-I cloud data with RTNEPH, ISCCP, and NMC MRF model cloud datasets have been made for two test cases. The preliminary results show that the

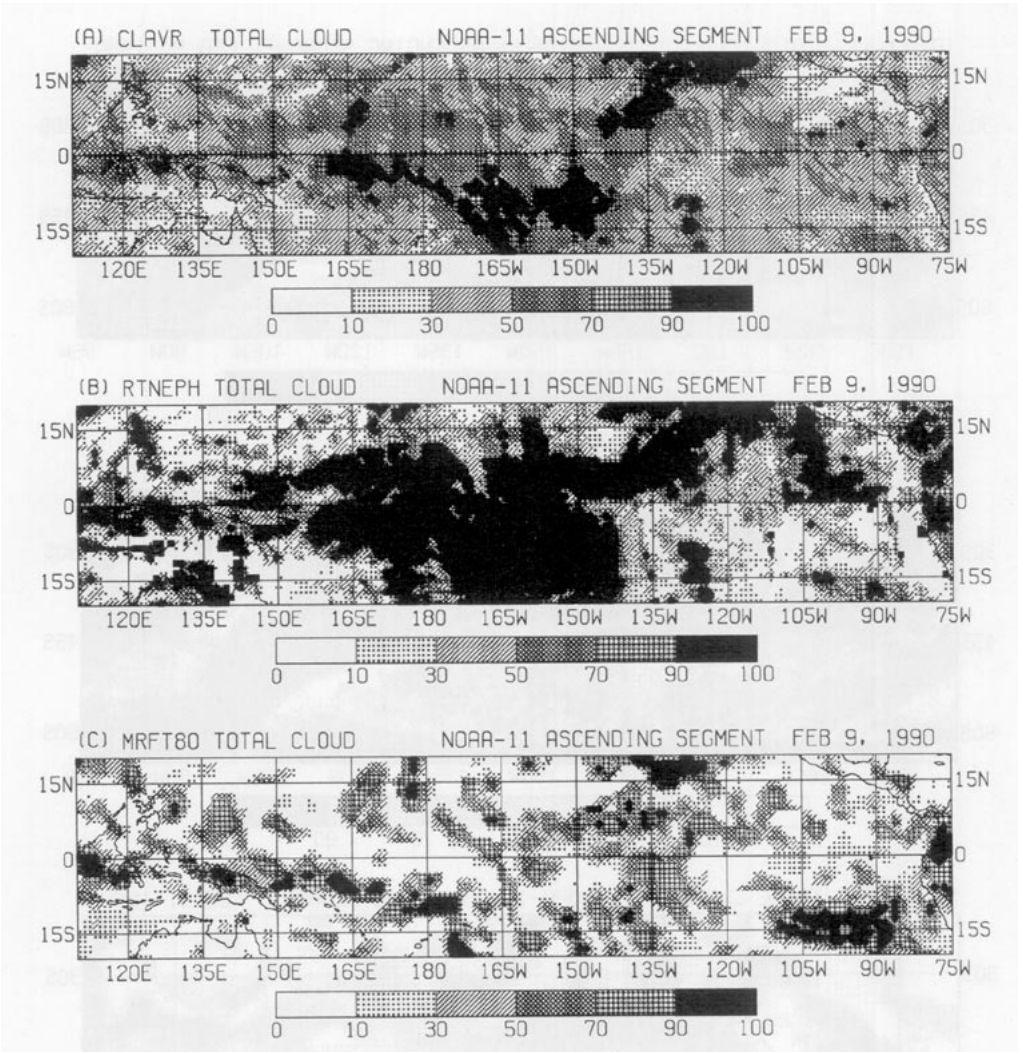

FIG. 8. Similar to Fig. 4 but for the tropical Pacific region.

CLAVR-I cloud data is capable of providing good global cloud distributions at high horizontal resolution. The main difficulty with the CLAVR-I product is its tendency to favor a cloud amount of 50%. Future work will improve the interpretation of mixed cloud conditions and provide a multilayer cloud analysis.

The current NMC MRF model cloud prediction scheme is capable of producing generally reasonable large-scale cloud patterns in midlatitudes, especially along frontal zones and storm tracks. However, even in midlatitude, several significant weaknesses are apparent. The model exhibits an early period spinup behavior, wherein the area-mean cloud amounts increase with time. Even following the spinup, the MRF area-mean cloud amounts show a significant negative bias, both in midlatitudes and the tropics. In lower latitudes, the model's cloud patterns are forced by the model's convective parameterization and compare poorly with the satellite retrievals. Here the model convective cloud clusters are too small and localized, reflecting characteristics of the model's tropical convective rainfall.

Statistical comparisons of model and "observed" clouds, presented in section 4, indicate that work is needed to improve the model's diagnosis of both cloud amount and location. The serious shortcomings result from imperfections in the model cloud parameterization scheme and in other model physical parameterizations, especially convection. There is active research at NMC to improve the model physical parameterizations and to develop a more physically based, explicit cloud scheme. In the context of diagnostic cloud schemes, Mitchell and Hahn (1989, 1990) present an automated, objective adjustment procedure (tuning) that eliminates model cloud forecast bias and cloud amount spinup in extratropical latitudes. In their scheme, cumulative frequency distributions of (a) observed layered cloud fraction (e.g., the RTNEPH cloud analysis) and (b) model forecast layer relative humidity

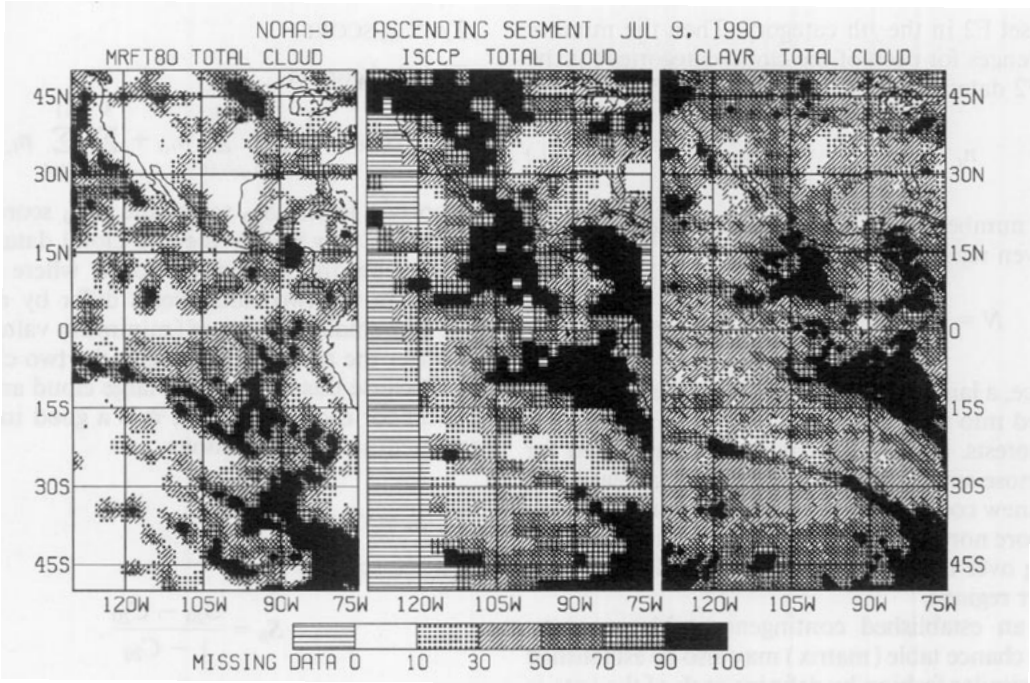

FIG. 9. Comparisons of total cloud amount distribution over the eastern Pacific, South to North American region. Data are mapped on *NOAA-9* satellite ascending segments of 9 July 1986.

are mapped one-to-one to yield critical relative humidity values and cloud-relative humidity functions. Their method is currently being tested with RTNEPH data at NMC. When CLAVR becomes operational, it will be used continuously to improve the model diagnostic cloud parameterization and data assimilation systems on a real-time basis.

Despite the inevitable differences between the three cloud analyses due to data sources, timeliness, and retrieval methods, these differences are significantly smaller than differences from MRF forecasts, showing that state of the art cloud analyses are of sufficient quality to improve cloud forecasts.

Acknowledgments. The authors wish to thank Captain John Pereira, U.S. Air Force Liaison Officer to NMC and NESDIS, for providing satellite orbiting information of the RTNEPH data used in this study. The authors would also like to thank Dr. Paul A. Davis of NESDIS, Dr. Peter M. Caplan of NMC, Capt. Norman H. Mandy of USAF, and three anonymous reviewers for their valuable comments and suggestions for improving this manuscript.

APPENDIX

Statistical Comparison Scores

The system of statistical comparison scores used in this study is adapted and modified from the one applied at AFGWC (Trapnell 1992). Score values are calculated from a set of cloud amount contingency tables. A brief description of the structure of a contingency table and definitions of comparison scores are given below.

a. Contingency table

Cloud amount has been divided into 11 categories over the entire cloud fraction range from 0 to 1. The interval value of cloud amount categories is 0.1 except a value of 0.05 is used at the two ends of the spectrum designated for clear sky and overcast conditions. For two compared cloud datasets, F1 versus F2, cloud groupings are denoted as $F1_i$ and $F2_j$ with i and j running from 1 to 11. A contingency table (or matrix) then is established for each of the specified geographic regions.

Contingency table:

	$F2_j$		
	$n_{1,1}$	. . . . .	$n_{1,11}$
	.	.	.
	.	.	.
$F1_i$	. . .	$n_{i,j}$	. . .
	.	.	.
	.	.	.
	$n_{11,1}$	. . . . .	$n_{11,11}$

Chance table:

	$F2_j$		
	$c_{1,1}$	. . . . .	$c_{1,11}$
	.	.	.
	.	.	.
$F1_i$	. . .	$c_{i,j}$	. . .
	.	.	.
	.	.	.
	$c_{11,1}$	. . . . .	$c_{11,11}$

An entry $n_{i,j}$ in the table represents the number of occurrences in the region that the first cloud dataset F1 falls in the ith cloud amount category and the sec-

ond dataset F2 in the jth category. Then the number of occurrences for each of the cloud categories for the F1 and F2 datasets is defined as follows:

$$n_i = \sum_{j=1}^{11} n_{i,j}, \quad n_j = \sum_{i=1}^{11} n_{i,j}. \tag{A1}$$

The total number of occurrences for all cloud categories in the given region will be:

$$N = \sum_{i=1}^{11} n_i = \sum_{j=1}^{11} n_j = \sum_{j=1}^{11} \sum_{i=1}^{11} n_{i,j}. \tag{A2}$$

In practice, a large region, such as the global area, may be divided into smaller regions focusing on particular study interests. Contingency tables are calculated for each of those smaller regions. Thus, one can easily establish a new contingency table for an area containing two or more nonoverlapping smaller regions by simply summing over the corresponding entries in the tables of smaller regions.

From an established contingency table, a corresponding chance table (matrix) may also be established in a very similar fashion by defining each of the entries as:

$$C_{i,j} = \frac{n_i n_j}{N} = N \frac{n_i}{N} \frac{n_j}{N} = NP_i P_j = NP_{i,j}, \tag{A3}$$

where $P_{i,j}$ may be interpreted as the joint probability on two statistically assumed independent databases, that one has clouds in the $\mathrm{F1}_i$ category while the other one has clouds in the $\mathrm{F2}_j$ category.

b. Statistical comparison scores

After establishing the contingency and corresponding chance tables, a number of useful statistical comparison scores can be derived. Listed below are some score definitions derived from a contingency table. A set of corresponding definitions of chance scores may also be obtained by simply replacing every $n_{i,j}$ in the definitions with the corresponding $c_{i,j}$ quantity.

1) S_{20} SCORE

The S_{20} score is

$$S_{20} = \frac{1}{N} \sum_{i=1}^{11} \sum_{\substack{j=i-1 \\ j \geq 1}}^{\substack{j \leq 11 \\ j=i+1}} n_{i,j}. \tag{A4}$$

The S_{20} score gives an estimate of how well two cloud datasets agree. Its value represents the fraction of points where the cloud amount in the two cloud fields differ by less than about 20%. The larger the score (maximum value is one), the better the agreement in cloud amount in a given area. Here a threshold value of 20% is set because, in most cases, exactly the same distribution from two different cloud data sources is not expected.

2) S_{-60} SCORE

The S_{60} score is

$$S_{-60} = \frac{1}{N} \left(\sum_{i=1}^{5} \sum_{j=i+6}^{11} n_{i,j} + \sum_{j=1}^{5} \sum_{i=j+6}^{11} n_{i,j} \right). \tag{A5}$$

In contrast to the S_{20} score, the S_{-60} score gives an estimate of how poorly the two cloud datasets agree. It represents the percent of points where the cloud amount in the two cloud fields differ by more than 60%. The smaller the score (minimum value is zero), the better the agreement between the two cloud datasets. Because this score tracks large cloud amount differences for each grid point, it is a good indicator of agreement in cloud locations.

3) S_h SCORE

The S_h score is

$$S_h = \frac{S_{20} - C_{20}}{1 - C_{20}}. \tag{A6}$$

The S_h score (called the Heidike score) is the relative difference between S_{20} and C_{20} (chance of S_{20} score). The score measures how closely the two cloud datasets are related to (or statistically dependent on) each other. In a perfect agreement between two cloud datasets, the S_{20} score is equal to 1, and in that limit, S_h approaches its maximum value of 1. The score is larger when the S_{20} score (i.e., actual frequency of occurrence of clouds within 20% difference for the two datasets) is far greater than the C_{20} score (i.e., chance of joint occurrence of two assumed statistically independent cloud datasets). The larger the S_h score, usually the better the agreement between two datasets.

4) ROOT-MEAN-SQUARE DIFFERENCE

The root-mean-square (rms) difference is

$$S_{\mathrm{rms}} = \left[\frac{1}{N} \sum_{j=1}^{11} \sum_{i=1}^{11} n_{i,j} (\mathrm{F1}_i - \mathrm{F2}_j)^2 \right]^{1/2}. \tag{A7}$$

In its definition, $\mathrm{F1}_i$ and $\mathrm{F2}_j$ are the mean values of cloud amount from the two datasets in the ith and jth cloud amount categories, respectively.

5) BIAS SCORE

The bias score is

$$S_{\mathrm{bias}} = \frac{1}{N} \sum_{j=1}^{11} \sum_{i=1}^{11} n_{i,j} (\mathrm{F1}_i - \mathrm{F2}_j). \tag{A8}$$

The bias score is useful in checking the difference (or bias) of overall mean cloud amount given by the two cloud datasets. A large positive (negative) value indicates that the overall mean cloud amount given by

dataset F1 is much larger (smaller) than that given by F2.

6) MEAN ABSOLUTE DIFFERENCE

The mean absolute difference is defined as

$$S_{\text{abs}} = \frac{1}{N}\sum_{j=1}^{11}\sum_{i=1}^{11} n_{i,j}|\text{F1}_i - \text{F2}_j|. \qquad \text{(A9)}$$

The S_{abs} score shows the mean magnitude of absolute differences of cloud amount between two datasets in a given area.

7) CORRELATION COEFFICIENT

The correlation coefficient is defined as

$$S_{\text{corr}} = \frac{\sigma_{xy}}{\sigma_x\sigma_y},$$

$$\sigma_{xy} = \frac{1}{N}\sum_{j=1}^{11}\sum_{i=1}^{11}[n_{i,j}(\text{F1}_i - \overline{\text{F1}})(\text{F2}_j - \overline{\text{F2}})],$$

$$\sigma_x = \left[\frac{1}{N}\sum_{i=1}^{11} n_i(\text{F1}_i - \overline{\text{F1}})^2\right]^{1/2},$$

$$\sigma_y = \left[\frac{1}{N}\sum_{j=1}^{11} n_j(\text{F2}_j - \overline{\text{F2}})^2\right]^{1/2}, \qquad \text{(A10)}$$

where

$$\overline{\text{F1}} = \frac{1}{N}\sum_{i=1}^{11} n_i\text{F1}_i, \quad \overline{\text{F2}} = \frac{1}{N}\sum_{j=1}^{11} n_j\text{F2}_j \qquad \text{(A11)}$$

are the average cloud amount values for the two cloud datasets. The higher the score value, the better the agreement in overall cloud patterns (amount and distribution) of the two cloud fields.

REFERENCES

Campana, K. A., 1990: Radiation and cloud parameterization at the National Meteorological Center. *Proc. ECMWF/WCRP Workshop on Clouds, Radiative Transfer and the Hydrological Cycle.* Reading, England, ECMWF, 313–340.

Coakley, J. A., Jr., and D. G. Baldwin, 1984: Towards the objective analysis of clouds from satellite imagery data. *J. Climate Appl. Meteor.*, **23,** 1065–1099.

Hamill, T. M., R. P. d'Entremont, and J. T. Bunting, 1992: A description of the air force real-time nephanalysis model. *Wea. Forecasting,* **7,** 288–306.

Henderson-Sellers, A., 1985: Layer cloud amount for January and July 1979 from 3D-nephanalysis. *J. Climate Appl. Meteor.*, **25,** 118–132.

Herman, G., M.-L. Wu, and W. Johnson, 1980: The effect of clouds on the earth's solar and infrared radiation budget. *J. Atmos. Sci.*, **37,** 1251–1261.

Kanamitsu, M., 1989: Description of the NMC global data assimilation and forecast system. *Wea. Forecasting,* **4,** 335–342.

Kiess, R. B., and W. M. Cox, 1988: The AFGWC automated real-time cloud analysis model. AFGWC/TN-88/001, Air Force Global Weather Central, Offutt AFB, NE, 82 pp.

Manabe, S., 1969: Climate and the ocean circulation: I. The atmospheric circulation and the hydrology of the earth's surface. *Mon. Wea. Rev.*, **97,** 739–774.

Mitchell, K. E., and D. C. Hahn, 1989: Development of a cloud forecast scheme for the GL baseline global spectral model. AFGL TR-89-0343, AFGL, Air Force Systems Command, Hanscom AFB, MA, 147 pp.

——, and ——, 1990: Objective development of diagnostic cloud forecast schemes in global and regional models. *Seventh Conf. on Atmospheric Radiation.* San Francisco, CA, Amer. Meteor. Soc., J138–J145.

Ramanathan, V., R. D. Cess, E. F. Harrison, P. Minnis, B. R. Barkstorm, and D. Hartman, 1989: Cloud-radiative forcing and climate: Results from the earth radiation budget experiment. *Science,* **243,** 57–63.

Rossow, W. B., E. Kinsella, A. Wolf, and L. Gardner, 1985: International Satellite Cloud Climatology Project (ISCCP): Description of reduced resolution radiance data. WMO/TD No. 58, World Meteorological Organization, Geneva, 132 pp.

Schiffer, R. A., and W. B. Rossow, 1983: The International Satellite Cloud Climatology Project (ISCCP): The first project of the World Climate Research Program. *Bull. Amer. Meteor. Soc.*, **64,** 779–784.

Slingo, J. M., 1980: A cloud parameterization scheme derived from GATE data for use with a numerical model. *Quart. J. Roy. Meteor. Soc.*, **106,** 747–770.

——, 1987: The development and verification of a cloud prediction scheme for the ECMWF model. *Quart. J. Roy. Meteor. Soc.*, **113,** 899–927.

Stephens, G. L., and T. J. Greenwald, 1991: The earth's radiation budget and its relation to atmospheric hydrology: 2. Observations of cloud effects. *J. Geophys. Res.*, **96,** 15 325–15 340.

Stowe, L. L., 1991: Cloud and aerosol products at NOAA/NESDIS. Palaeoclimatol., Palacoecol. [Global and Planetary Change section], **90,** 25–32.

——, H. Y. M. Yeh, T. F. Eck, C. G. Wellemeyer, H. L. Kyle, and the *Nimbus-7* Cloud Data Processing Team, 1989: *Nimbus-7* global cloud climatology, Part II: First year results. *J. Climate,* **2,** 671–709.

——, E. P. MaClain, R. Carey, P. Pellegrino, G. Gutman, P. Davis, C. Long, and S. Hart, 1991: Global distribution of cloud cover derived from NOAA/AVHRR operational satellite data. *Adv. Space Res.*, **11,** 51–54.

Sundqvist, H., E. Berge, and J. Kristjansson, 1989: Condensation and cloud parameterization studies with a mesoscale numerical weather prediction model. *Mon. Wea. Rev.*, **117,** 1641–1657.

Trapnell, R. N., Jr., 1992: Cloud curve algorithm test program. Rep. PL-TR-92-2052, Phillips Lab., Hanscom AFB, MA, 170 pp.

Wilson, C. A., and J. F. B. Mitchell, 1986: Diurnal variation and cloud in a general circulation model. *Quart. J. Roy. Meteor. Soc.*, **112,** 347–369.

Zamiska, A., 1986: *RTNEPH USAFETAC Climatic Database Users Handbook No. 1.* USAFETAC/User Handbook-86/001, USAF Environmental Technical Applications Center, Operating Location A, Asheville, N.C., 15 pp.